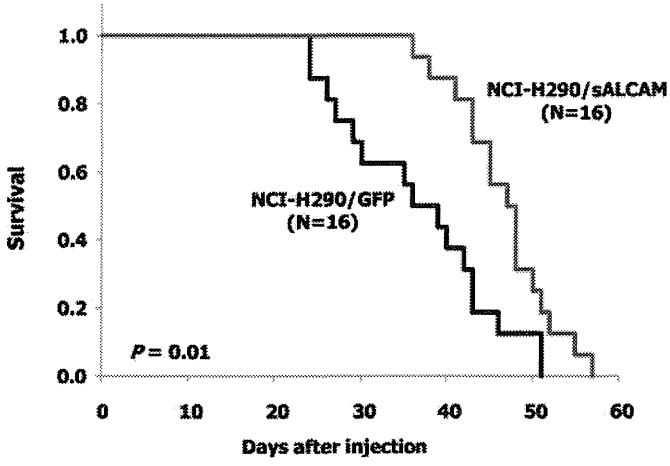

FIGURE 6. MM cells with sALCAM expression showed longer survival in vivo. Nude mice were injected with MM cell lines infected with NCI-H290/sALCAM or NCI-H290/GFP (1×10^6) virus into the right thoracic cavity. NCI-H290/sALCAM group showed a significantly prolonged survival ($p = 0.01$ and log-rank test). MM, malignant mesothelioma; sALCAM, soluble activated leukocyte cell-adhesion molecule.

impaired the migration of melanoma cells and diminished lung metastases of melanoma cells in vivo. Thus, their results suggested that sALCAM may also act as a tumor suppressor for the tumor cells with ALCAM expression. As we also showed the inhibitory effect of sALCAM on MM cells, we considered sALCAM to possibly have a therapeutic potential for MM.

ALCAM has also been shown to be a target molecule for immunotherapeutic modality against human cancers. For example, an internalizing single-chain antibody fragment directed to ALCAM, which was conjugated to immunoliposomal cytotoxic agents was shown to effectively target and kill ALCAM-expressing ovarian-cancer and prostate-cancer cells in vitro.[52,53] Wiiger et al[54] also demonstrated the potential role of a human recombinant anti-ALCAM antibody as a therapeutic agent against colon and breast cancers. Thus, these newly developed immunotherapeutic agents might also be beneficial for MM treatment.

In conclusion, our study revealed that overexpression of ALCAM contributes positively to MM progression and that sALCAM effectively inhibits tumor progression. We considered that ALCAM might be a potential therapeutic target of MM. Further investigation about the detailed mechanisms of how cell migration, invasion. and anchorage-independent growth can be enhanced in MM cells by ALCAM is also needed to provide new insights into a more effective strategy to target the ALCAM expressed on MM cells.

ACKNOWLEDGMENTS

We thank Ms. Mika Yamamoto and Ms. Yasue Matsudaira for their excellent technical assistance and Professor Yuichi Ueda (Department of Cardiothoracic Surgery, Nagoya University Graduate School of Medicine, Japan) for his encouragement of this study.

REFERENCES

1. Carbone M, Bedrossian CW. The pathogenesis of mesothelioma. *Semin Diagn Pathol* 2006;23:56–60.
2. Pass HI, Vogelzang N, Hahn S, Carbone M. Malignant pleural mesothelioma. *Curr Probl Cancer* 2004;28:93–174.
3. Ramos-Nino ME, Testa JR, Altomare DA, et al. Cellular and molecular parameters of mesothelioma. *J Cell Biochem* 2006;98:723–734.
4. Robinson BW, Lake RA. Advances in malignant mesothelioma. *N Engl J Med* 2005;353:1591–1603.
5. Tsao AS, Wistuba I, Roth JA, Kindler HL. Malignant pleural mesothelioma. *J Clin Oncol* 2009;27:2081–2090.
6. Vogelzang NJ, Rusthoven JJ, Symanowski J, et al. Phase III study of pemetrexed in combination with cisplatin versus cisplatin alone in patients with malignant pleural mesothelioma. *J Clin Oncol* 2003;21:2636–2644.
7. Weder W, Stahel RA, Bernhard J, et al.; Swiss Group for Clinical Cancer Research. Multicenter trial of neo-adjuvant chemotherapy followed by extrapleural pneumonectomy in malignant pleural mesothelioma. *Ann Oncol* 2007;18:1196–1202.
8. Krug LM, Pass HI, Rusch VW, et al. Multicenter phase II trial of neoadjuvant pemetrexed plus cisplatin followed by extrapleural pneumonectomy and radiation for malignant pleural mesothelioma. *J Clin Oncol* 2009;27:3007–3013.
9. de Perrot M, Feld R, Cho BC, et al. Trimodality therapy with induction chemotherapy followed by extrapleural pneumonectomy and adjuvant high-dose hemithoracic radiation for malignant pleural mesothelioma. *J Clin Oncol* 2009;27:1413–1418.
10. Yilmaz M, Christofori G, Lehembre F. Distinct mechanisms of tumor invasion and metastasis. *Trends Mol Med* 2007;13:535–541.
11. Schmalhofer O, Brabletz S, Brabletz T. E-cadherin, beta-catenin, and ZEB1 in malignant progression of cancer. *Cancer Metastasis Rev* 2009;28:151–166.
12. King JE, Thatcher N, Pickering CA, Hasleton PS. Sensitivity and specificity of immunohistochemical markers used in the diagnosis of epithelioid mesothelioma: a detailed systematic analysis using published data. *Histopathology* 2006;48:223–232.
13. Sato A, Torii I, Okamura Y, et al. Immunocytochemistry of CD146 is useful to discriminate between malignant pleural mesothelioma and reactive mesothelium. *Mod Pathol* 2010;23:1458–1466.
14. Orecchia S, Schillaci F, Salvio M, Libener R, Betta PG. Aberrant E-cadherin and gamma-catenin expression in malignant mesothelioma and its diagnostic and biological relevance. *Lung Cancer* 2004;45 Suppl 1:S37–S43.
15. Ito A, Hagiyama M, Mimura T, et al. Expression of cell adhesion molecule 1 in malignant pleural mesothelioma as a cause of efficient adhesion and growth on mesothelium. *Lab Invest* 2008;88:504–514.
16. Bidlingmaier S, He J, Wang Y, et al. Identification of MCAM/CD146 as the target antigen of a human monoclonal antibody that recognizes both epithelioid and sarcomatoid types of mesothelioma. *Cancer Res* 2009;69:1570–1577.
17. Nelissen JM, Peters IM, de Grooth BG, van Kooyk Y, Figdor CG. Dynamic regulation of activated leukocyte cell adhesion molecule-mediated homotypic cell adhesion through the actin cytoskeleton. *Mol Biol Cell* 2000;11:2057–2068.
18. Bowen MA, Patel DD, Li X, et al. Cloning, mapping, and characterization of activated leukocyte-cell adhesion molecule (ALCAM), a CD6 ligand. *J Exp Med* 1995;181:2213–2220.
19. Weidle UH, Eggle D, Klostermann S, Swart GW. ALCAM/CD166: cancer-related issues. *Cancer Genomics Proteomics* 2010;7:231–243.
20. Whitney GS, Starling GC, Bowen MA, Modrell B, Siadak AW, Aruffo A. The membrane-proximal scavenger receptor cysteine-rich domain of CD6 contains the activated leukocyte cell adhesion molecule binding site. *J Biol Chem* 1995;270:18187–18190.
21. Bowen MA, Bajorath J, Siadak AW, et al. The amino-terminal immunoglobulin-like domain of activated leukocyte cell adhesion molecule binds specifically to the membrane-proximal scavenger receptor cysteine-rich domain of CD6 with a 1:1 stoichiometry. *J Biol Chem* 1996;271:17390–17396.
22. Zimmerman AW, Joosten B, Torensma R, Parnes JR, van Leeuwen FN, Figdor CG. Long-term engagement of CD6 and ALCAM is essential for T-cell proliferation induced by dendritic cells. *Blood* 2006;107:3212–3220.

23. Ibáñez A, Sarrias MR, Farnós M, et al. Mitogen-activated protein kinase pathway activation by the CD6 lymphocyte surface receptor. *J Immunol* 2006;177:1152–1159.
24. Degen WG, van Kempen LC, Gijzen EG, et al. MEMD, a new cell adhesion molecule in metastasizing human melanoma cell lines, is identical to ALCAM (activated leukocyte cell adhesion molecule). *Am J Pathol* 1998;152:805–813.
25. van Kempen LC, Nelissen JM, Degen WG, et al. Molecular basis for the homophilic activated leukocyte cell adhesion molecule (ALCAM)-ALCAM interaction. *J Biol Chem* 2001;276:25783–25790.
26. Ikeda K, Quertermous T. Molecular isolation and characterization of a soluble isoform of activated leukocyte cell adhesion molecule that modulates endothelial cell function. *J Biol Chem* 2004;279:55315–55323.
27. Swart GW. Activated leukocyte cell adhesion molecule (CD166/ALCAM): developmental and mechanistic aspects of cell clustering and cell migration. *Eur J Cell Biol* 2002;81:313–321.
28. Heffron DS, Golden JA. DM-GRASP is necessary for nonradial cell migration during chick diencephalic development. *J Neurosci* 2000;20:2287–2294.
29. van Kempen LC, van den Oord JJ, van Muijen GN, Weidle UH, Bloemers HP, Swart GW. Activated leukocyte cell adhesion molecule/CD166, a marker of tumor progression in primary malignant melanoma of the skin. *Am J Pathol* 2000;156:769–774.
30. Lunter PC, van Kilsdonk JW, van Beek H, et al. Activated leukocyte cell adhesion molecule (ALCAM/CD166/MEMD), a novel actor in invasive growth, controls matrix metalloproteinase activity. *Cancer Res* 2005;65:8801–8808.
31. van Kilsdonk JW, Wilting RH, Bergers M, et al. Attenuation of melanoma invasion by a secreted variant of activated leukocyte cell adhesion molecule. *Cancer Res* 2008;68:3671–3679.
32. Weichert W, Knösel T, Bellach J, Dietel M, Kristiansen G. ALCAM/CD166 is overexpressed in colorectal carcinoma and correlates with shortened patient survival. *J Clin Pathol* 2004;57:1160–1164.
33. Ishigami S, Ueno S, Arigami T, et al. Clinical implication of CD166 expression in gastric cancer. *J Surg Oncol* 2011;103:57–61.
34. Kahlert C, Weber H, Mogler C, et al. Increased expression of ALCAM/CD166 in pancreatic cancer is an independent prognostic marker for poor survival and early tumour relapse. *Br J Cancer* 2009;101:457–464.
35. King JA, Ofori-Acquah SF, Stevens T, Al-Mehdi AB, Fodstad O, Jiang WG. Activated leukocyte cell adhesion molecule in breast cancer: prognostic indicator. *Breast Cancer Res* 2004;6:R478–R487.
36. Tomita K, van Bokhoven A, Jansen CF, et al. Activated leukocyte cell adhesion molecule (ALCAM) expression is associated with poor prognosis for bladder cancer patients. *UroOncology* 2003;3:121–129.
37. Mezzanzanica D, Fabbi M, Bagnoli M, et al. Subcellular localization of activated leukocyte cell adhesion molecule is a molecular predictor of survival in ovarian carcinoma patients. *Clin Cancer Res* 2008;14:1726–1733.
38. Verma A, Shukla NK, Deo SV, Gupta SD, Ralhan R. MEMD/ALCAM: a potential marker for tumor invasion and nodal metastasis in esophageal squamous cell carcinoma. *Oncology* 2005;68:462–470.
39. Sawhney M, Matta A, Macha MA, et al. Cytoplasmic accumulation of activated leukocyte cell adhesion molecule is a predictor of disease progression and reduced survival in oral cancer patients. *Int J Cancer* 2009;124:2098–2105.
40. Usami N, Fukui T, Kondo M, et al. Establishment and characterization of four malignant pleural mesothelioma cell lines from Japanese patients. *Cancer Sci* 2006;97:387–394.
41. Kawaguchi K, Murakami H, Taniguchi T, et al. Combined inhibition of MET and EGFR suppresses proliferation of malignant mesothelioma cells. *Carcinogenesis* 2009;30:1097–1105.
42. King JA, Tan F, Mbeunkui F, et al. Mechanisms of transcriptional regulation and prognostic significance of activated leukocyte cell adhesion molecule in cancer. *Mol Cancer* 2010;9:266.
43. Murakami H, Mizuno T, Taniguchi T, et al. LATS2 is a tumor suppressor gene of malignant mesothelioma. *Cancer Res* 2011;71:873–883.
44. Altomare DA, Menges CW, Pei J, et al. Activated TNF-alpha/NF-kappaB signaling via down-regulation of Fas-associated factor 1 in asbestos-induced mesotheliomas from Arf knockout mice. *Proc Natl Acad Sci USA* 2009;106:3420–3425.
45. Sekido Y. Genomic abnormalities and signal transduction dysregulation in malignant mesothelioma cells. *Cancer Sci* 2010;101:1–6.
46. van Kilsdonk JW, van Kempen LC, van Muijen GN, Ruiter DJ, Swart GW. Soluble adhesion molecules in human cancers: sources and fates. *Eur J Cell Biol* 2010;89:415–427.
47. Koch AE, Halloran MM, Haskell CJ, Shah MR, Polverini PJ. Angiogenesis mediated by soluble forms of E-selectin and vascular cell adhesion molecule-1. *Nature* 1995;376:517–519.
48. Bowen MA, Aruffo AA, Bajorath J. Cell surface receptors and their ligands: in vitro analysis of CD6-CD166 interactions. *Proteins* 2000;40:420–428.
49. Gho YS, Kleinman HK, Sosne G. Angiogenic activity of human soluble intercellular adhesion molecule-1. *Cancer Res* 1999;59:5128–5132.
50. Gho YS, Kim PN, Li HC, Elkin M, Kleinman HK. Stimulation of tumor growth by human soluble intercellular adhesion molecule-1. *Cancer Res* 2001;61:4253–4257.
51. Morbidelli L, Brogelli L, Granger HJ, Ziche M. Endothelial cell migration is induced by soluble P-selectin. *Life Sci* 1998;62:PL7–P11.
52. Piazza T, Cha E, Bongarzone I, et al. Internalization and recycling of ALCAM/CD166 detected by a fully human single-chain recombinant antibody. *J Cell Sci* 2005;118(Pt 7):1515–1525.
53. Roth A, Drummond DC, Conrad F, et al. Anti-CD166 single chain antibody-mediated intracellular delivery of liposomal drugs to prostate cancer cells. *Mol Cancer Ther* 2007;6:2737–2746.
54. Wiiger MT, Gehrken HB, Fodstad Ø, Maelandsmo GM, Andersson Y. A novel human recombinant single-chain antibody targeting CD166/ALCAM inhibits cancer cell invasion in vitro and in vivo tumour growth. *Cancer Immunol Immunother* 2010;59:1665–1674.

IJC
International Journal of Cancer

The circadian clock gene *BMAL1* is a novel therapeutic target for malignant pleural mesothelioma

Momen Elshazley[1], Mitsuo Sato[1], Tetsunari Hase[1], Ryo Yamashita[1], Kenya Yoshida[1], Shinya Toyokuni[2], Futoshi Ishiguro[3,4], Hirotaka Osada[3], Yoshitaka Sekido[3], Kohei Yokoi[4], Noriyasu Usami[4], David S. Shames[5], Masashi Kondo[1], Adi F. Gazdar[6], John D. Minna[6] and Yoshinori Hasegawa[1]

[1] Department of Respiratory Medicine, Nagoya University Graduate School of Medicine, Japan
[2] Department of Pathology and Biological responses, Nagoya University Graduate School of Medicine, Japan
[3] Division of Molecular Oncology, Aichi Cancer Center Research Institute, Japan
[4] Department of Thoracic Surgery, Nagoya University Graduate School of Medicine, Japan
[5] Department of Oncology Diagnostics, Genentech Inc., South San Francisco, CA
[6] Hamon Center for Therapeutic Oncology Research, University of Texas Southwestern Medical Center at Dallas, 6000 Harry Hines, Dallas, TX

Malignant pleural mesothelioma (MPM) is a highly aggressive neoplasm arising from the mesothelial cells lining the parietal pleura and it exhibits poor prognosis. Although there has been significant progress in MPM treatment, development of more efficient therapeutic approaches is needed. *BMAL1* is a core component of the circadian clock machinery and its constitutive overexpression in MPM has been reported. Here, we demonstrate that *BMAL1* may serve as a molecular target for MPM. The majority of MPM cell lines and a subset of MPM clinical specimens expressed higher levels of *BMAL1* compared to a nontumorigenic mesothelial cell line (MeT-5A) and normal parietal pleural specimens, respectively. A serum shock induced a rhythmical *BMAL1* expression change in MeT-5A but not in ACC-MESO-1, suggesting that the circadian rhythm pathway is deregulated in MPM cells. *BMAL1* knockdown suppressed proliferation and anchorage-dependent and independent clonal growth in two MPM cell lines (ACC-MESO-1 and H290) but not in MeT-5A. Notably, *BMAL1* depletion resulted in cell cycle disruption with a substantial increase in apoptotic and polyploidy cell population in association with downregulation of Wee1, cyclin B and $p21^{WAF1/CIP1}$ and upregulation of cyclin E expression. *BMAL1* knockdown induced mitotic catastrophe as denoted by disruption of cell cycle regulators and induction of drastic morphological changes including micronucleation and multiple nuclei in ACC-MESO-1 cells that expressed the highest level of *BMAL1*. Taken together, these findings indicate that *BMAL1* has a critical role in MPM and could serve as an attractive therapeutic target for MPM.

Key words: apoptosis, *BMAL1*, mesothelioma, targeted therapy, mitotic catastrophe

Abbreviations: BMAL1: brain and muscle ARNT-like protein-1; STR: short tandem repeat; GAPDH: glyceraldehyde 3-phosphate dehydrogenase; BSS: balanced salt solution; H–E: Hematoxlin and Eosin; HEPES: 4-2-hydroxyethyl-1-piperazineetha-nesulfonic acid; MPM: malignant pleural mesothelioma; NPAS2: neuronal PAS domain protein 2; qRT-PCR: quantitative real-time reverse transcriptase-PCR; siRNA: short interfering RNA; DAPI: 4,6-diamidino-2-phenylindole

Additional Supporting Information may be found in the online version of this article.

DOI: 10.1002/ijc.27598
History: Received 25 Dec 2011; Accepted 23 Mar 2012; Online 17 Apr 2012

Correspondence to: Mitsuo Sato, Department of Respiratory Medicine, Nagoya University Graduate School of Medicine, 65 Tsurumai-cho, Showaku, Nagoya, Aichi 466-8550, Japan, Tel.: +81-52-744-2167, Fax: +81-52-744-2176, E-mail: msato@med.nagoya-u.ac.jp

Malignant pleural mesothelioma (MPM) is a highly aggressive neoplasm arising from the mesothelial or submesothelial cells lining the parietal pleura. MPM has a particularly poor prognosis with a median survival of approximately 12 months from the onset of diagnosis.[1] Asbestos exposure is considered the most important etiologic factor that has been mentioned in relation to MPM.[2] Although a significant progress in MPM treatment has been achieved, there is an urgent need for developing new therapeutic approaches to improve the clinical outcome of patients with MPM.[3]

Many physiological, biological and metabolic processes are controlled by a homeostatic system called the circadian clock. This system is regulated by a circadian pacemaker located in the suprachiasmatic nucleus of the anterior hypothalamus that controls peripheral clocks over the 24 hr.[4] Recent studies have shown that peripheral tissues also have advanced molecular mechanisms that regulate circadian events, many of which have also been observed in established cell lines.[5–7]

Several circadian clock genes have been reported to control circadian rhythms in peripheral tissues, including three period proteins (PER1, PER2 and PER3), two cryptochromes (CRY1 and CRY2), CLOCK, NPAS2 and BMAL proteins. *BMAL1* is an indispensible core component in the circadian

clock machinery. It can form heterodimer complexes with *CLOCK* or *NPAS2* genes; this complex drives transcription from E-box elements found in the promoters of circadian-responsive genes.[8] Period and cryptochrome proteins negatively regulate CLOCK/BMAL1 dimer-mediated transcription, thereby forming the feedback loop that regulates the timing of clock gene transcription.[9]

Disruption of the circadian clock has been associated with a wide variety of human disorders including cancer.[10] Previous studies have shown that clock genes are involved in the pathogenesis of human cancers. These genes seem to function primarily as tumor suppressors.[11] Several studies have reported the involvement of *BMAL1* in human cancers. High *BMAL1* expression was associated with poor patients' prognosis and distant metastasis in colorectal and breast cancer.[12,13] In addition, vascular endothelial growth factor is transcriptionally upregulated by *BMAL1*.[14] These reports suggest an oncogenic role for *BMAL1*. By contrast, Taniguchi *et al.*[4] showed that *BMAL1* expression is inactivated by promoter methylation in hematologic malignancies but not in solid cancers and that exogenously overexpressed *BMAL1* suppresses *in vitro* and *in vivo* growth of a lymphoma cell line, indicating a tumor suppressive role of *BMAL1* that may be specific for hematologic malignancies.

Recently, expression microarray analysis of MPM showed overexpression of several circadian rhythm genes compared to normal parietal pleural. Specifically, the *BMAL1* transcript was found to be overexpressed in MPM whereas negative regulators of *BMAL1* were expressed at lower levels. These findings raise the possibility that *BMAL1* could contribute to the aggressive malignant phenotypes of MPM.[15] To the best of our knowledge, no prior studies have analyzed the functional roles of *BMAL1* in MPM and thus we sought to investigate the role of *BMAL1* in the pathogenesis of MPM and its potential utility as a therapeutic target for MPM.

Material and Methods

Cell lines and tissue culture

Thirteen MPM cell lines and a nontumorgenic mesothelial cell line (MeT-5A) were used in this study. We purchased H2452, H2052, MSTO-211H, H28 and MeT-5A cell lines from the American Type Culture Collection and confirmed their authenticity by short tandem repeat (STR) analysis. H290 and H2373 were gifts from Dr Adi F. Gazdar (University of Texas Southwestern Medical Center, Dallas, TX). ACC-MESO-1, Y-MESO-12, Y-MESO-9, ACC-MESO-4, Y-MESO-22 (epithelioid) Y-MESO-14 (biphasic), and Y-MESO-8D (sarcomatoid) cell lines are established by ourselves.[16] Cells were grown in monolayer cultures in RPMI 1640 (Sigma-Aldrich Corp., St. Louis, MO, USA) containing 10% fetal bovine serum, 2 mmol/L glutamine and 1 mmol/L sodium pyruvate at 37°C in a humidified atmosphere of 95% air and 5% CO_2. MeT-5A cells were cultured in Medium 199 with Earle's balanced salt solution, 0.75 mM L-glutamine and 1.25 g/L sodium bicarbonate supplemented with 3.3 nM epidermal growth factor, 400 nM hydrocortisone, 870 nM insulin, 20 mM 4-2-hydroxyethyl-1-piperazineetha-nesulfonic acid and 10% fetal bovine serum.

RNA isolation and quantitative real-time reverse transcriptase-PCR analysis

For mRNA analysis, 5 μg of total RNA isolated using Trizol (Invitrogen, Carlsbad, CA, USA) were reverse transcribed with Super script III First-Strand Synthesis System using Random primer system (Invitrogen, Carlsbad, CA, USA). Quantitative real-time reverse transcriptase-PCR (qRT-PCR) analysis of *BMAL1*, *NPAS2* and *CLOCK* was performed as described previously.[17] GAPDH (Assays-on-Demand; Applied Biosystems, Foster City, CA, USA) was used as an internal control.

Transfection of short interfering RNA

Cells (4.5×10^5) were plated in 10 cm^2 dish plate. Next day, cells were transiently transfected with either 10 nM predesigned short interfering RNA (siRNA) [Stealth Select RNA interference (RNAi)] targeting *BMAL1* or control siRNA purchased from Invitrogen using Lipofectamine RNAiMAX (Invitrogen Corp., Carlsbad, CA, USA) according to the manufacturer's protocol. After 48 hr, the transfected cells were harvested for further analysis or plated for growth assays.

Western blot analysis

Cells were collected and washed twice in 1× phosphate-buffered saline (PBS), then lysed in ice-cold lysis buffer (0.5 M Tris-HCl with pH 7.4, 1.5 M NaCl, 2.5% deoxycholic acid, 10 mM EDTA, 10% NP-40, 0.5 mM DTT, 1 mM phenylmethylsulfonyl fluoride, 5 mg/mL leupeptin and 10 mg/mL aprotinin) for 5 min. The lysate was centrifuged at 13,000 rpm for 20 min at 4°C, and protein content of the supernatant was measured. Total cell lysates (30 μg/well) were separated by SDS-PAGE and the gels transferred into nitrocellulose membranes (Whatman, Piscataway, NJ). Membranes were blocked with 5% nonfat dry milk in PBS containing Tween-20 (PBST) (1× PBS, 0.1% Tween-20) for 1 hr at room temperature and incubated with primary antibody at 4°C overnight. Membranes were then washed three times with PBST and probed with appropriate horseradish peroxidase-conjugated secondary antibody for 1 hr at room temperature. The membranes were washed three times in PBST and bands were visualized using Western blot chemiluminescence reagent (BioRad, Hercules, CA 94547, USA). Antibodies were obtained from Santa Cruz (CA. 95060, USA) and Cell Signaling (Danvers, MA 01923, USA) Biotechnologies and used at the following dilutions (BMAL1, 1:1,000; Cyclin B, 1:1,000; Cyclin E, 1:1,000; Wee1, 1:1,000; $p21^{WAF1/CIP1}$, 1:1,000; Cleaved caspase 3, 1:1,000; beta-actin, 1:5,000).

Immunofluorescence staining

Forty-eight-hour post-transfection with *BMAL1*-siRNA or control-siRNA oligos, *in vitro* growing cells were seeded at 2×10^4 cells/chamber in two-well Lab-Tek™ Chamber Slide System, incubated overnight at 37°C and 5% CO_2. Next day, cells were washed with PBS and fixed with 4% paraformaldehyde

solution, permeabilized with 0.01% Triton X-100 and blocked in 1% BSA in PBS for 20 min at room temperature. Subsequent antibody incubations were in PBS containing 1% BSA–0.01% Triton X-100. Antibody reagents were mouse anti-α-tubulin (1:100, Sigma-Aldrich St. Louis, MO, USA) and rabbit anti-BMAL1 H-170 (1:200, Santa Cruz Biotechnology, CA. 95060, USA). Incubation with primary antibody was kept overnight at 4°C, followed by three washes with PBS solution. Secondary reagent with Alexa Flour® 488-cojugated goat antimouse IgG, goat antirabbit IgG (1:1,000, Molecular probes, Invitrogen, Eugene, OR 97402, USA) and Alexa Flour® 594-cojugated goat antimouse IgG (1:700, Molecular probes, Invitrogen Eugene, OR 97402, USA). Secondary antibodies were incubated for 1 hr at room temperature. After PBS washing, independent mounting was done with Prolong Gold antifade reagent supplemented with 4,6-diamidino-2-phenylindole (DAPI) (Invitrogen, Carlsbad, CA, USA). All stained cells were visualized by confocal Eclipse TE 2000-E microscope (Nikon, Tokyo, Japan) with 20×, 40× and 60× objectives.

Tumor specimens of patients with MPM

Sixteen resected MPM tissue specimens were obtained from patients diagnosed with MPM who underwent surgery at the Department of Thoracic Surgery, Nagoya University Hospital between 2005 and 2011. Eleven patients received neoadjuvant chemotherapy with pemetrexed and cisplatin, while one patient received adjuvant chemotherapy and radiotherapy. Fifteen specimens were obtained through extra-pleural pneumonectomy and one was obtained by pleurectomy. Diagnosis of mesothelioma was made based on clinical evaluation, histopathologic examination, and the clinical stage was determined according to the International Mesothelioma Interest Group.[18] Patients' overall survival was defined as the length of time from the date of surgery to that of death. Four noncancerous (normal parietal pleura) tissue specimens were obtained from patients who underwent thoracic surgery for different causes (*i.e.*, not including mesothelioma) and were used as normal controls. The study protocol was approved by the Institutional Review Boards of Nagoya University Graduate School of Medicine. Informed consent was obtained from the patients following institutional guidelines. The expression level of the circadian clock protein, *BMAL1*, was examined in the aforementioned surgically resected specimens. Sections from formalin-fixed paraffin-embedded were treated for immunostaining with commercially available BMAL1 antibody (Sanata Cruz Biotechnology, CA.95060, USA) according to the procedures described elsewhere.[13]

Cell growth assays

Colorimetric proliferation assay was performed using WST-1 assay kit (Roche, Basel, Switzerland) according to manufacturer's instruction. Liquid and soft agar colony formation assays were done as described previously.[19]

Cell cycle analysis

Post-transfection with *BMAL1*-siRNA or control oligos, cells were synchronized by serum starvation for 12 hr or by double-thymidine treatment (to block mitosis and induce late G1/early S phase arrest; subconfluent cell cultures were incubated in complete medium containing 2 mM thymidine for 18 hr, and then, the thymidine medium was removed and replaced with complete medium lacking thymidine for 12 hr followed by another 18-hr incubation in the presence of thymidine). Synchronized populations were harvested and washed in ice-cold PBS. Following centrifugation at 900*g* for 5 min, cells were suspended in 150 μL of cold PBS while vortex gently, and cells were fixed by dropwise addition of 350 μL ice-cold ethanol. Fixed cells were stored at −20°C for at least 30 min. For staining, pelleted cells were washed twice with cold PBS and resuspended in 0.5 mL PBS containing 200 μg/mL RNase, and stained with propidium iodide 20 μg. Cells were incubated at 37°C for 30 min and maintained at 4°C before analysis, cells were filtered through 40 μM nylon mesh and analyzed by flow cytometry for cell cycle status [FACS Calibur instrument (Becton Dickinson), with BD Cell Quest™ Pro Ver. 5.2.1 (BD) Bioscience, Franklin Lakes, NJ, USA].

Apoptosis analysis

Apoptosis was quantified by detecting surface exposure of phosphatidylserine in apoptotic cells using a phycoerythrin (PE)—Annexin V Apoptosis Detection Kit I (BD Biosciences). Cells were harvested 5 days after transfection of siRNA oligos, treated according to the manufacturer's instructions and measured with PE 7-amino-actinomycin D (7-AAD) staining using flow cytometry [FACS Calibur instrument (Becton Dickinson), with BD Cell Quest™ Pro Ver. 5.2.1 (BD) Bioscience, Franklin Lakes, NJ, USA].

Hematoxylin and eosin staining

Post-transfection with *BMAL1*-siRNA or control oligos, ACC-MESO-1 cells were harvested after 48 hr and 10,000 cells were plated/chambered in eight-well Lab-Tek™ Chamber Slide System, and then incubated overnight at 37°C and 5% CO_2. Next day, cells washed with PBS and fixed with 1% glutaraldehyde for 5 min and subsequently stained with Mayer's Hematoxylin solution (Muto Puro Chemical LTD, Tokyo, Japan) for 2–3 min, rinsed with distilled water and then submerged in Scott's tap water substitute (0.2% $NaHCO_3$ and 2% $MgSO_4$) for bluing, finally cells were washed with distilled water once and examined under the microscope.

Statistics

SPSS Ver. 18 software was used for all statistics analysis in this study. Mann–Whitney *U*-test was used for analyzing difference between two groups.

Results

MPM cell lines express higher levels of *BMAL1* than normal pleural mesothelial cells

Quantitative detection of *BMAL1* and *NPAS2* mRNA in a panel of MPM and MeT-5A cell lines was performed using qRT-PCR. Ten out of 13 (77%) MPM cell lines expressed

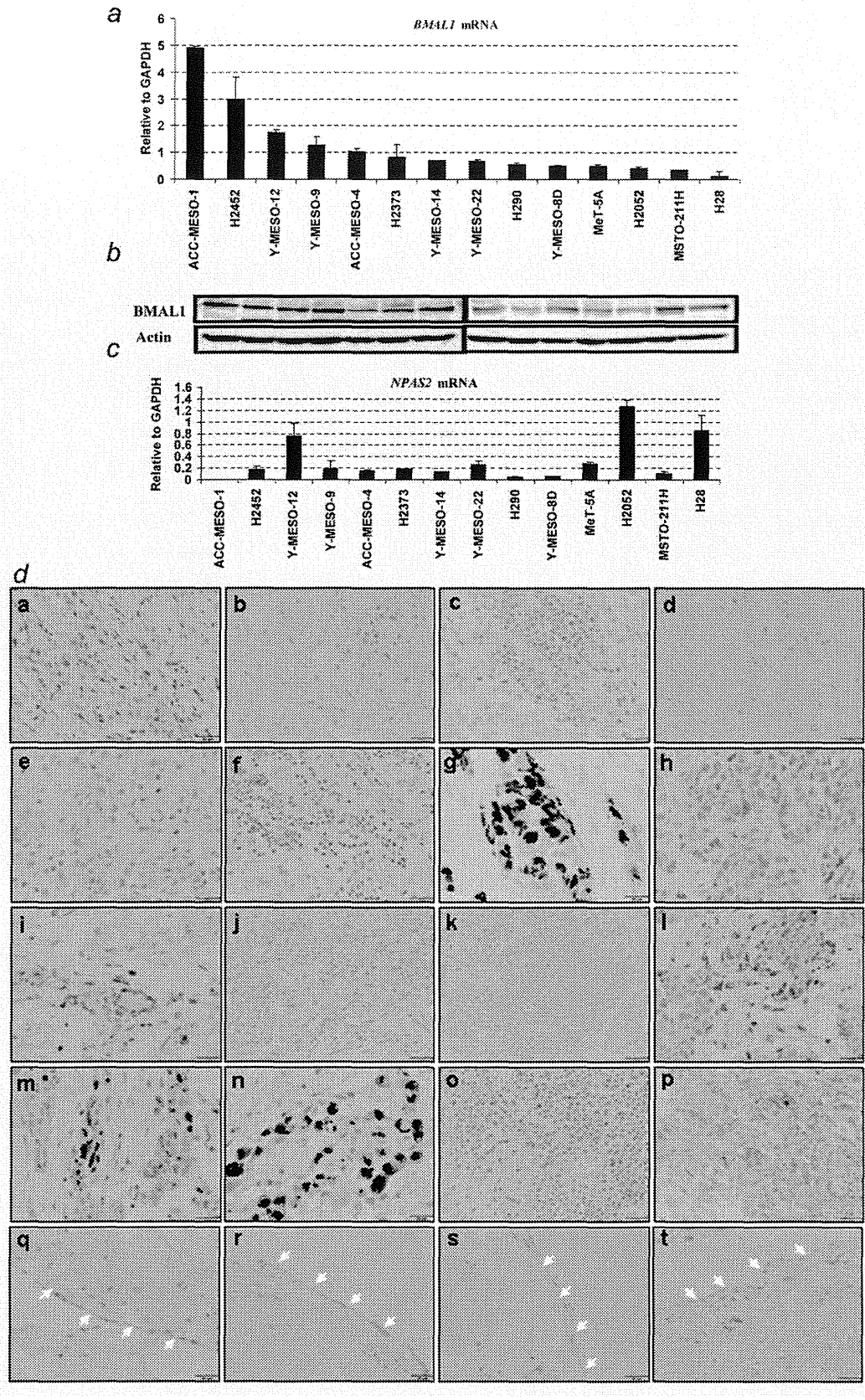

Figure 1. *BMAL1* expression levels in MPM and normal parietal pleura. (*a*) qRT-PCR analysis of *BMAL1* in 13 MPM cell lines and an immortalized pleural mesothelial cell line MeT-5A (control). The cell lines are aligned by expression levels of *BMAL1* mRNA from high (left) to low (right). The result is a representative of two independent qRT-PCR experiments done in duplicated reactions. (*b*) Western blots of *BMAL1* in MPM cell lines. Actin was used as a loading control. (*c*) qRT-PCR analysis of *NPAS2* in 13 MPM cell lines and MeT-5A. (*d*) Immunohistochemical staining of BMAL1 in surgically annotated MPM and normal parietal pleural specimens. Immunohistochemical analysis showed an overexpression of BMAL1 in a subset of MPM specimen (a–p), whereas normal pleural mesothelial cells showed negative BMAL1 immunoreactivity (white arrows, q–t). Details of MPM and normal parietal pleural specimens were mentioned in "Material and Methods" Section. ×400 magnification and 25 μm scale bars were used for all images. [Color figure can be viewed in the online issue, which is available at wileyonlinelibrary.com.]

Table 1. Clinical features of 16 patients with MPM

ID	Age/Sex	Histology	BMAL1 Status (IHC score)	Asbestos exposure	OS (M)	Staging		Surgery	Therapy
						Clinical	Pathological		
1	50/M	Biphasic	Negative (1+)	+	2.5	T2N0M0/II	T3N2M0/III	Right EPP	No
2	54/M	Biphasic	Negative (1+)	+	24.0	T2N0M0/II	T2N0M0/II	Left EPP	No
3	56/M	Epithelioid	Negative (1+)	+	25.3	T3N2M0/III	T4N0M0/IV	Left EPP	No
4	65/M	Epithelioid	Negative (0)	+	8.8	T3N1M0/III	T3N2M0/III	Right EPP	Neoadjuvant CT
5	46/F	Epithelioid	Negative (1+)	−	36.0	T1bN0M0/Ib	T3N2M0/III	Left EPP	Adjuvant CT + LRT
6	70/F	Epithelioid	Negative (0)	−	27.6	T1bN1M0/III	T2N1M0/III	Left EPP	Neoadjuvant CT
7	65/M	Epithelioid	Positive (3+)	+	8.4	T3N0M0/III	T4N0M0/IV	Right EPP	Neoadjuvant CT
8	60/M	Biphasic	Negative (0)	+	31.3	T3N2M0/III	T3N0M0/III	Right EPP	Neoadjuvant CT + PHR
9	62/M	Epithelioid	Positive (2+)	+	13.0	T3N0M0/III	T4NxM0/IV	Left pleurectomy	Neoadjuvant CT
10	67/M	Biphasic	Negative (1+)	−	11.6	T2N1M0/III	T3N0M0/III	Right EPP	Neoadjuvant CT + PHR
11	66/M	Biphasic	Negative (0)	+	8.3	T2N0M0/II	T3N0M0/III	Right EPP	Neoadjuvant CT
12	67/M	Epithelioid	Positive (2+)	+	3.6	T2N0M0/II	T3N2M0/III	Right EPP	No
13	68/M	Epithelioid	Positive (3+)	−	7.7	T3N0M0/III	T3N0M0/III	Left EPP	Neoadjuvant CT + PHR
14	63/M	Epithelioid	Positive (3+)	+	1.9	T2N0M0/II	T3N0M0/III	Lt EPP	Neoadjuvant CT
15	68/M	Sarcomatoid	Negative (0)	+	1.0	T3N2M0/III	T3N0M0/III	Right EPP	Neoadjuvant CT
16	64/M	Epithelioid	Negative (1+)	+	0.8	T2N0M0/II	T3N2M0/III	Left EPP	Neoadjuvant CT

Abbreviations: Id, patient's number; IHC, immunohistochemical score for *BMAL1*; OS, overall survival; M, month; EPP, extra-pleural pneumonectomy; neoadjuvant CT, neoadjuvant chemotherapy (cisplatin + pemetrexed); adjuvant chemotherapy (cisplatin + pemetrexed); LRT, local radiation therapy; PHR, post-operative hemithoracic radiation.

higher levels of *BMAL1* mRNA than MeT-5A, while *NPAS2* expression profile seems different from *BMAL1* profile in MPM cell lines (Figs. 1*a* and 1*c*). Western blot analysis for the same set of cell lines clearly demonstrated variable degrees of BMAL1 protein expression (Fig. 1*b*). Furthermore, we investigated *BMAL1* expression levels in 16 surgically annotated MPM and four normal parietal pleural specimens (Table 1). Through immunohistochemical analysis, BMAL1 was detected in a subset of MPM specimens with nuclear and/or cytoplasmic localization, while none of the four normal parietal pleural samples showed detectable levels of BMAL1 protein (Fig. 1*d*), suggesting that BMAL1 may be important in the development of MPM.

Expression profile of *BMAL1* and *CLOCK* over 24 hr in ACC-MESO-1 and MeT-5A cells

Based on previous data showing that expression of BMAL1 followed a rhythmical pattern in animal models,[20] we decided to examine the expression of *BMAL1* and *CLOCK* by qRT-PCR analysis to evaluate their oscillation over 24 hr in ACC-MESO-1 and MeT-5A cells. We used the mouse fibroblast cell line (NIH3T3) as a positive control as it shows a rhythmical expression of BMAL1.[20] Serum shock was done as described previously.[5] *BMAL1* rhythmical expression was found in serum-shocked normal nontumorigenic mesothelial cells but not in ACC-MESO-1 cells, whereas *CLOCK* showed rhythmical expression in both MPM and normal mesothelial cells (Fig. 2). These findings indicate that *BMAL1* rhythmical expression was intact in normal mesothelial cells but not in MPM cells.

BMAL1 knockdown suppresses proliferation, anchorage-dependent and independent clonal growth of MPM cells

To investigate the role of *BMAL1* in MPM cell growth, we performed RNAi-mediated gene silencing against *BMAL1*. ACC-MESO-1 and H290 cell lines were selected as the MPM cell models to be used for further investigations (Fig. 1*a*). MeT-5A was used as a normal control. To reduce the off target effects, we used low dose (10 nM) stealth selected RNAi (Invitrogen Carlsbad, CA, USA) which includes three siRNA oligos with nonoverlapping sequences targeting *BMAL1*. Efficient *BMAL1* knockdown was confirmed by qRT-PCR, western blotting and immunostaining (Fig. 3). Next, to evaluate the effect of *BMAL1* knockdown on cell proliferation in mass culture and clonogenic growth in anchorage-dependent and independent conditions, we performed colorimetric growth, liquid and soft agar colony formation assays. We found that in ACC-MESO-1 and H290 cells, *BMAL1* knockdown significantly suppressed proliferation and dramatically suppressed colony formation in anchorage-dependent (liquid colony formation assay) and anchorage-independent conditions (soft agar assay) (Fig. 4). By contrast, we did not see significant suppression of proliferation in MeT-5A (Supporting Information, Fig. S1*a*).

BMAL1 depletion induces massive apoptosis in MPM cells, with limited consequences in the normal pleural mesothelial cells

Next, we investigated whether the antiproliferative effect of *BMAL1* depletion is due to cell death. *BMAL1* knockdown resulted in massive apoptosis and necrosis in MPM cells (Fig. 5*a*), as evidenced by increases in cleaved caspase-3 activation

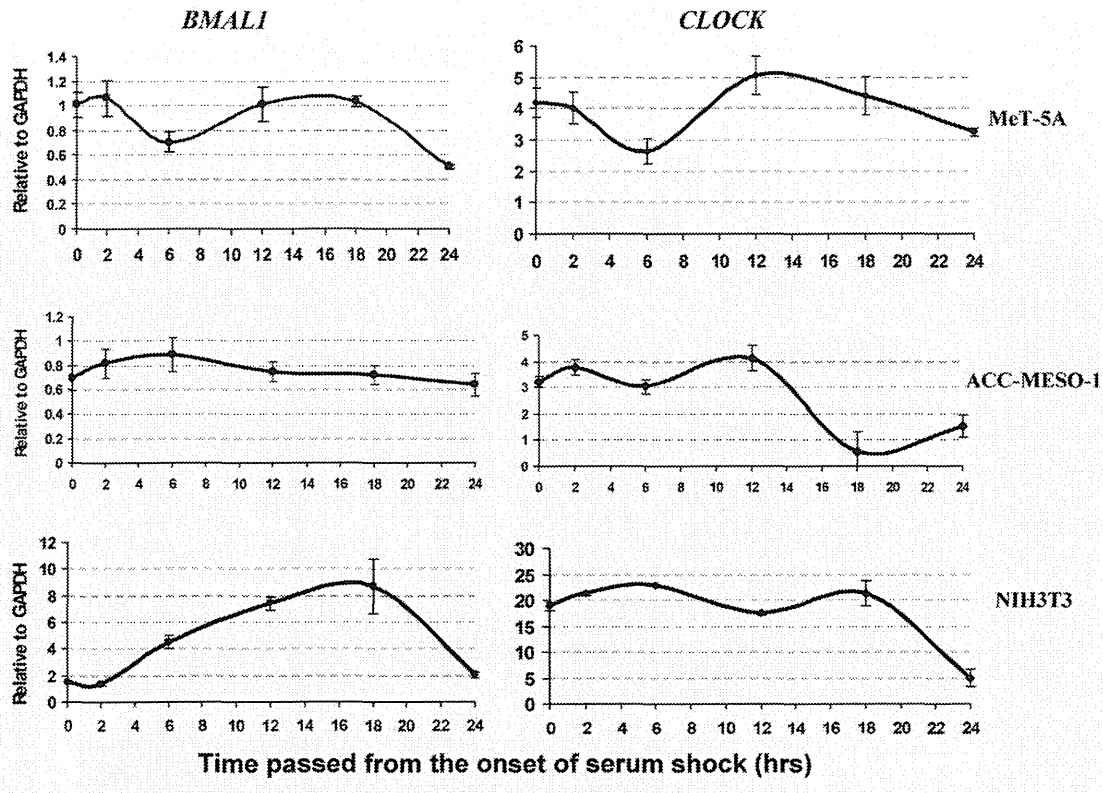

Figure 2. Expression profiles of *BMAL1* and *CLOCK* genes over 24 hr in ACC-MESO-1 and MeT-5A cells. qRT-PCR analysis of *BMAL1* and *CLOCK* mRNA in ACC-MESO-1, MeT-5A at time indicated above. NIH3T3 cells were used as a positive control. Serum shock was performed as mentioned in the "Materials and Methods" Section. We found that serum shock induces rhythmical expression changes of *BMAL1* and *CLOCK* mRNA in NIH3T3 as well as MeT-5A cells. Serum shocked ACC-MESO-1 cells showed rhythmical changes of *CLOCK* mRNA, but not *BMAL1* (GAPDH was used as an internal control). The results are averages of two independent experiments done in duplicate.

in ACC-MESO-1 cells (Fig. 5*b*). By contrast, subtle apoptosis could be found in MeT-5A cells following *BMAL1* knockdown (Fig. 5*a*). These results indicate that *BMAL1* knockdown-induced growth inhibition occurs in part through apoptotic mechanisms and MPM cells are more dependent on *BMAL1* expression for their survival than normal mesothelial cells.

BMAL1 knockdown leads to cell cycle disruption in ACC-MESO-1 cells with a clear rise of polyploidy

We investigated whether *BMAL1* knockdown-induced growth inhibition also was caused by cell cycle arrest. Consistent with induction of apoptosis as measured by cleaved caspase-3 expression, there was an increase in subG1 DNA content in ACC-MESO-1 transfected with *BMAL1*-siRNA oligos compared to cells transfected with control oligos (Fig. 5*c*). The proportion of cells in G1 phase decreased whereas a modest increase in the proportion of cells in G2/M phase. Notably, the profiling also showed an increase in the fraction of cells whose DNA contents exceed 4 *N* that correspond to polyploidy cell population. With much longer times in culture, high percentages of those cells (in G2/M phase and polyploidy region) decreased while subG1 population significantly increased (Fig. 5*c*), implying that polyploidy cells underwent apoptosis. By contrast, we did not see significant changes in cell cycle profiling of MeT-5A following *BMAL1* knockdown (Supporting Information, Fig. S1*b*).

Depletion of *BMAL1* induces drastic morphological alterations indicative of mitotic catastrophe in ACC-MESO-1 cells

We noted that following *BMAL1* knockdown, ACC-MESO-1 cells underwent drastic morphological changes; the cells enlarged and elongated by visual examination under phase contrast microscopy. Next, we performed hematoxlin and eosin (H–E) staining for these cells. As shown in Figure 6*a*, dramatic morphological alterations were seen in ACC-MESO-1 cells after *BMAL1* knockdown; cells exhibit much enlarged flattened shape, micronucleation, multiple nuclei and vacuolization occasionally were found. Next, we examined *BMAL1* siRNA-treated ACC-MESO-1 cells by detailed morphological analysis of DAPI-stained cell nuclei and α-tubulin immunostaining to visualize the cytoskeletal alterations associated with changes in nuclear morphology. Multiple morphological defects were identified which are consistent with the findings observed by H–E staining (Figs. 6*b* and

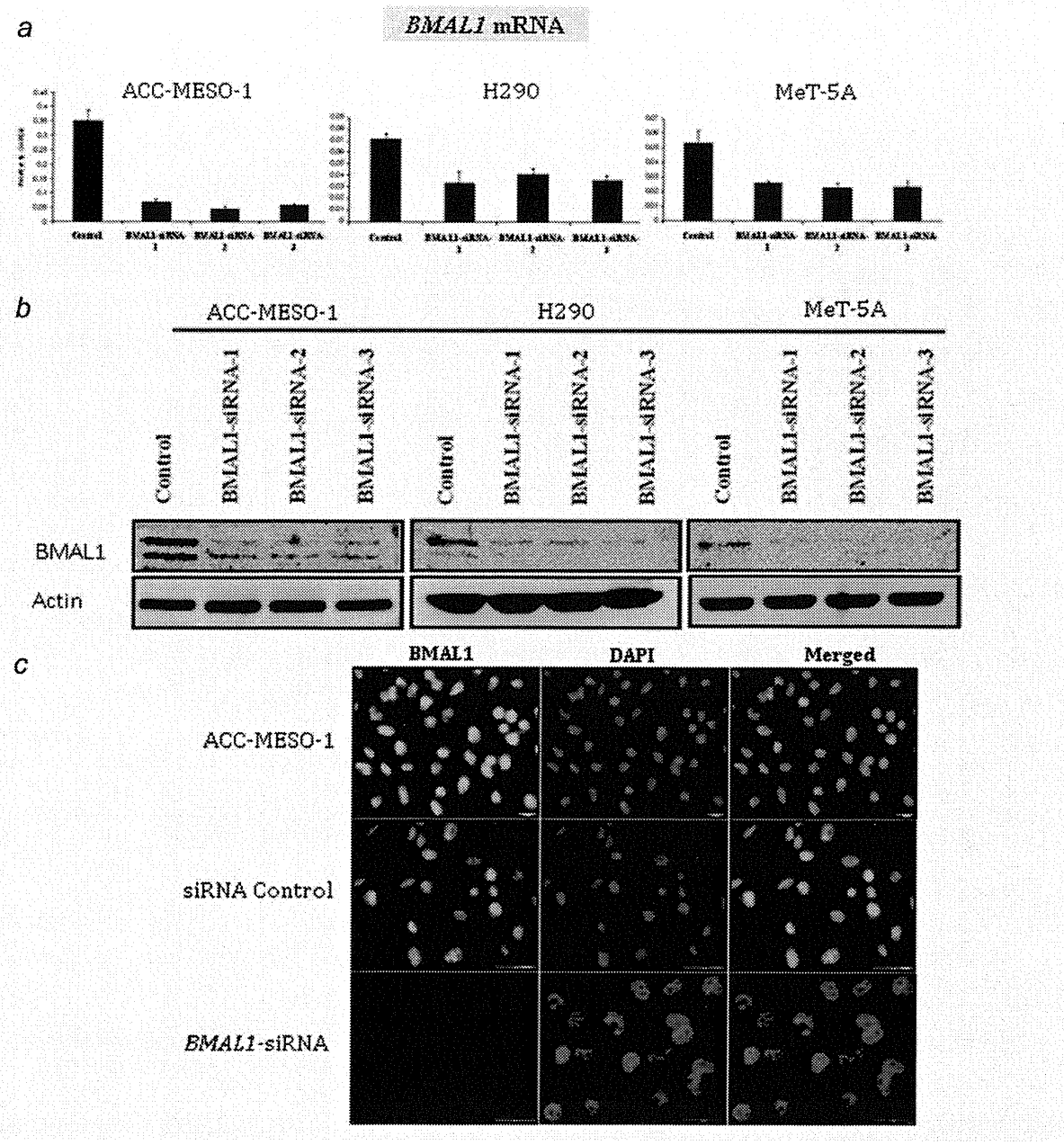

Figure 3. *BMAL1* knockdown in MPM and MeT-5A cells. Confirmation of *BMAL1* knockdown by (*a*) qRT-PCR, (*b*) Western blot analysis and (*c*) immunofluorescence (IF) assay. IF was used to examine BMAL1 levels in the parental, siRNA control or siRNA-BMAL1-treated ACC-MESO-1 cells. All data are averages of three independent experiments done in duplicates. [Color figure can be viewed in the online issue, which is available at wileyonlinelibrary.com.]

6*c*). Importantly, the existence of micronucleation is a highly indicative sign of catastrophic mitosis. To examine the possibility of mitotic catastrophe as a sequel of *BMAL1* knockdown and to explain its role in *BMAL1*-induced cell death during the cell cycle, ACC-MESO-1 cells transfected with *BMAL1*-siRNA or control oligos synchronized using a double thymidine block (to induce pharmacological block of mitosis in these cells). Interestingly, inhibition of mitosis in ACC-MESO-1 transfected with *BMAL1* siRNA resulted in a marked decrease of polyploidy and subG1 population (Fig. 6*d*), suggesting aberrant mitosis as a cause of cell death after BMAL1 knockdown. To confirm the occurrence of mitotic catastrophe following *BMAL1* knockdown, we performed time lapse microscopic examination for ACC-MESO-1 cells transfected with *BMAL1*-siRNA or control oligos. Examination showed that cells rounding up as they entered mitosis, then attempting to undergo cytokinesis. ACC-MESO-1 cells transfected with control siRNA successfully completed mitosis, but *BMAL1* siRNA-treated cells failed to divide properly and exhibited large cell volume and micronucleation (Fig. 6*e*), indicating mitotic catastrophe as a cell fate following BMAL1 knockdown in those cells.

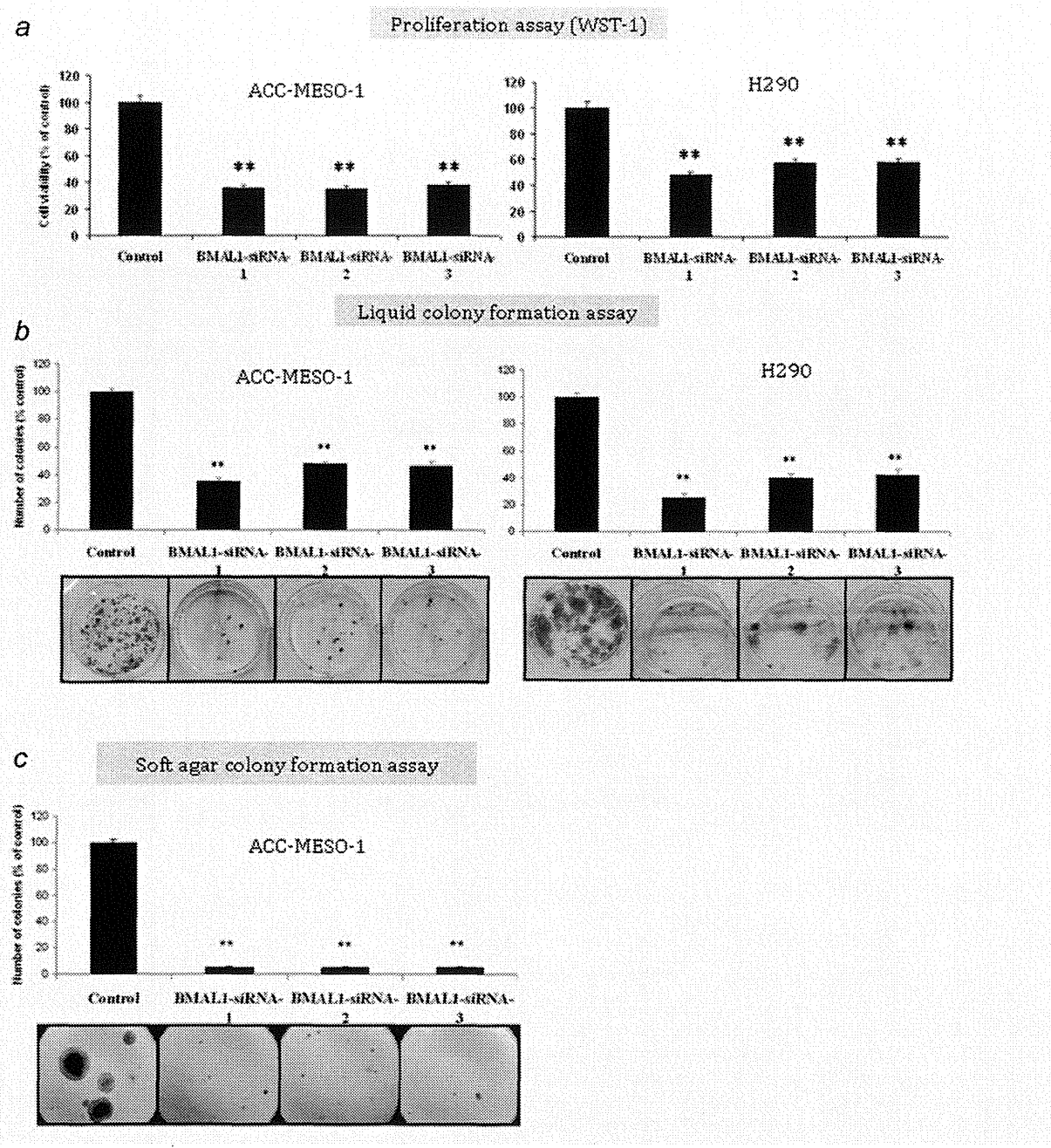

Figure 4. *BMAL1* knockdown inhibits proliferation and suppresses clonal growth of MPM cells in anchorage-dependent and -independent conditions. (*a*) WST-1 proliferation. (*b*) Liquid colony formation assays for ACC-MESO-1 and H290 cells transfected with BMAL1-siRNA or control oligos. (*c*) Soft agar colony formation assay for ACC-MESO-1 cells transfected with BMAL1-siRNA or control oligos. Results are from three independent experiments and shown as mean ± SD. In liquid colony and soft agar assay colony, numbers of cells transfected with control oligos are set as 100%. ** indicate $p < 0.01$ (Mann–Whitney *U* test). All data are averages of three independent experiments done in duplicates. [Color figure can be viewed in the online issue, which is available at wileyonlinelibrary.com.]

RNAi-mediated knockdown of *BMAL1* results in expression alterations of the cell cycle regulators in ACC-MESO-1 cells

Recent data suggest that there is a strong relationship between the circadian clock system and regulation of the cell cycle.[21,22] In particular, *BMAL1* is considered a key regulator of cancer cell proliferation through coordinating the activity of cell cycle proteins including $p21^{WAF1/CIP1}$ and cyclin B. Specifically, some data suggest that the circadian clock controls mitotic process through Wee1, known to be clock target gating the G2/M transition.[10,21,23] Therefore, we investigated the link between *BMAL1* knockdown and the status of the cell cycle proteins. Notably, ACC-MESO-1 cells after *BMAL1* knockdown showed profound alterations in cell cycle

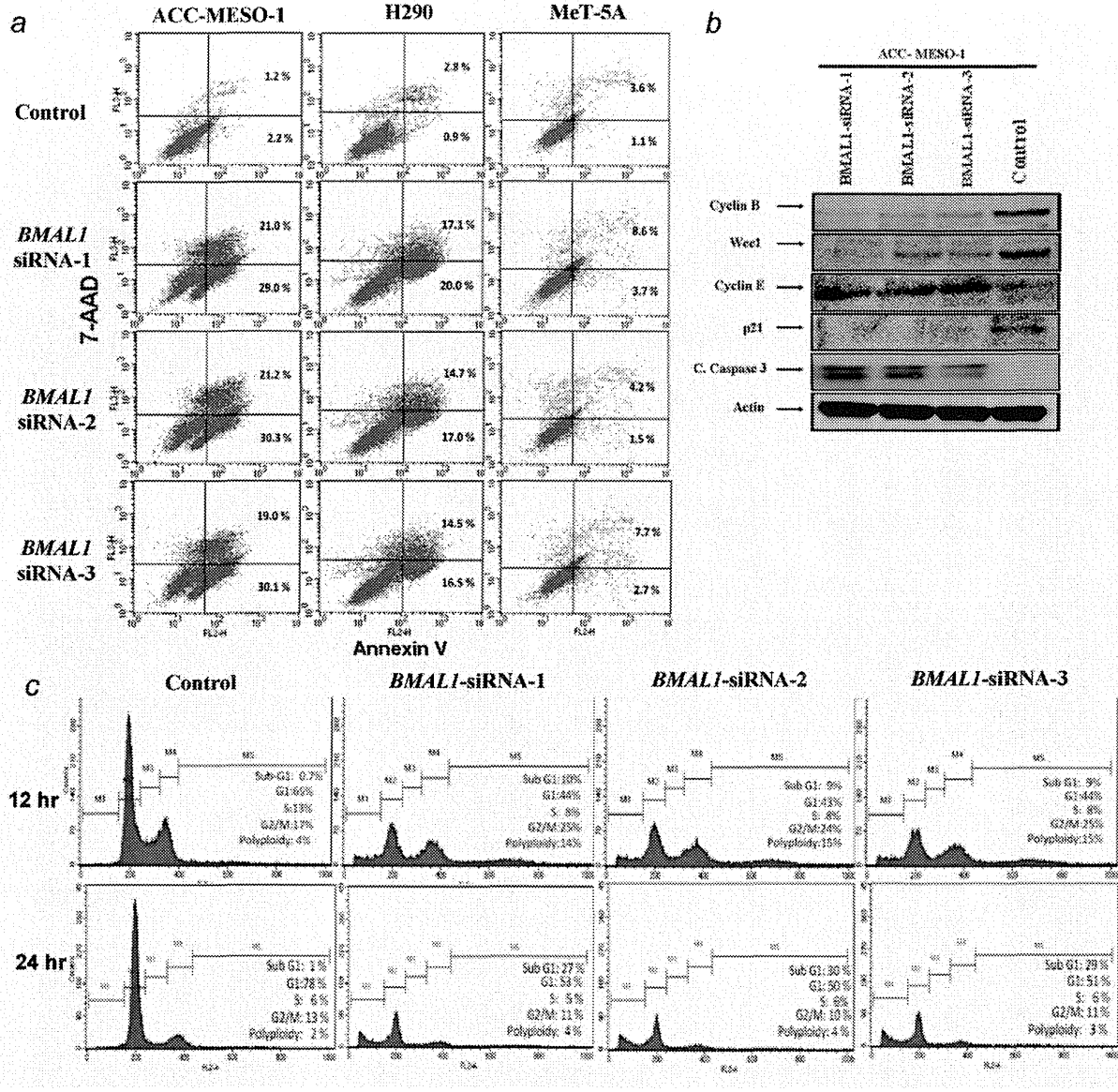

Figure 5. *BMAL1* knockdown induces apoptosis and cell cycle disruption (*a*) FACS analysis of cells costained with anti-annexin V and 7-AAD. High Annexin V and low 7-AAD cells are undergoing apoptosis while cells with low Annexin and high 7-AAD are undergoing necrosis. (*b*) Immunoblot showing effects of *BMAL1* knockdown on its targets in ACC-MESO-1 cells. (*c*) Cell cycle analysis of ACC-MESO-1 cells transfected with *BMAL1*-siRNA or control oligos. Forty-eight-hour post-transfection cells underwent serum starvation for 12 hr (upper panel) and for 24 hr (lower panel) then were harvested with both adherent and floating cells were combined and prepared for cell cycle analysis by flow cytometry, as described in "Material and Methods" Section. Results are the average of two independent experiments. [Color figure can be viewed in the online issue, which is available at wileyonlinelibrary.com.]

regulators, including significant decrease of Wee1, $p21^{WAF1/CIP1}$, cyclin B proteins and accumulation of cyclin E protein (Fig. 5*b*).

Discussion

In this report, we show that most MPM cell lines and a subset of surgically annotated MPM specimens expressed higher levels of *BMAL1* than MeT-5A and normal parietal pleural specimens, respectively. Silencing of *BMAL1* resulted in suppression of MPM cell growth and induction of apoptosis in these cells but limited effect was observed in MeT-5A. *BMAL1* depletion from ACC-MESO-1 cells, which expressed the highest level of *BMAL1*, led to cell cycle disruption with a substantial increase in apoptotic and polyploidy cell population as well as decreased levels of Wee1, cyclin B and $p21^{WAF1/CIP1}$ expression and upregulation of cyclin E. *BMAL1* knockdown in ACC-MESO-1 cells induced mitotic catastrophe denoted by marked disruption of cell cycle regulator proteins and drastic morphological changes including micronucleation, multiple nuclei and increased cellular volume of ACC-MESO-1 cells.

By immunohistochemical analysis, we demonstrated that *BMAL1* is constitutively expressed in a subset of clinical

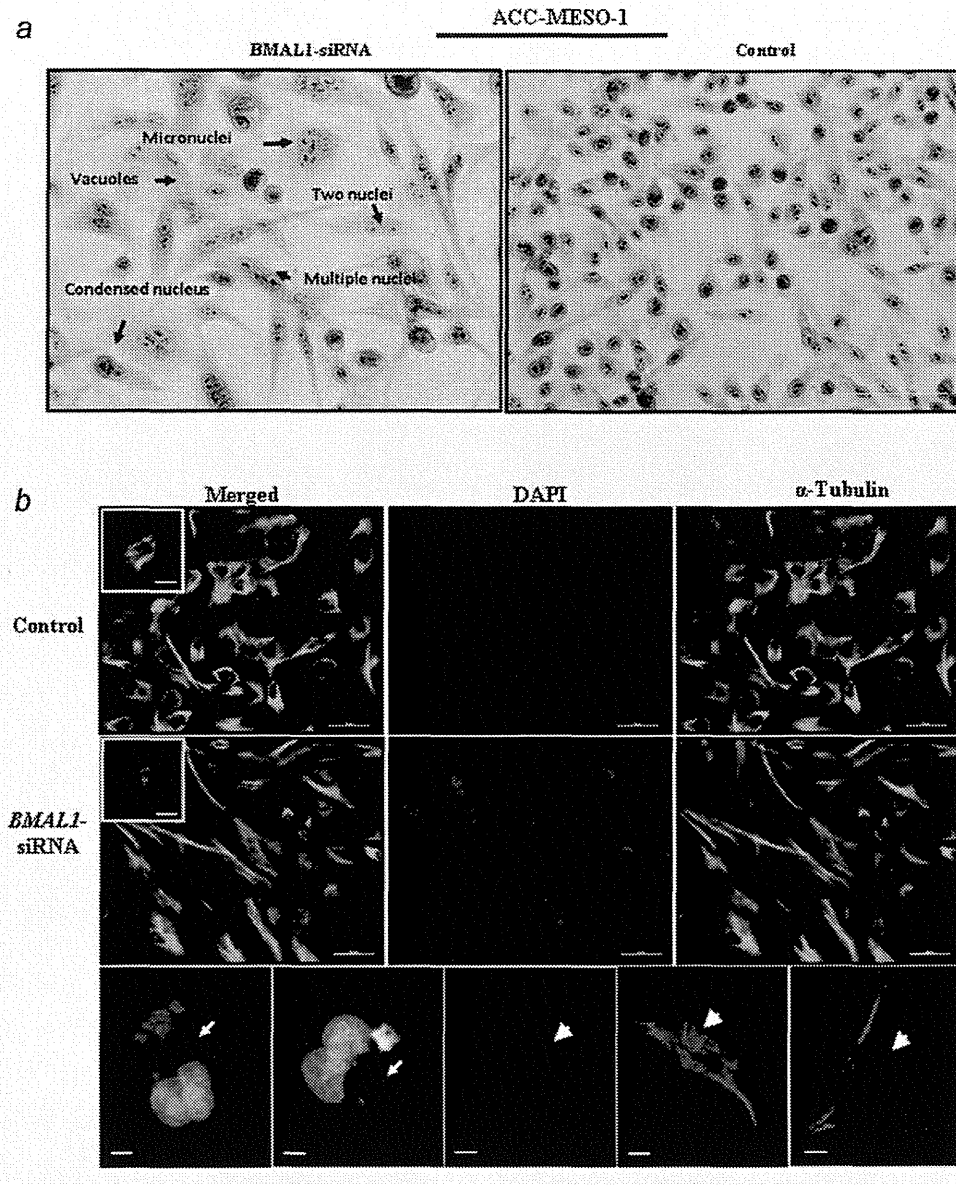

Figure 6. *BMAL1* knockdown induces dramatic morphological alterations in ACC-MESO-1 cells. (*a*) H–E stain showing the nuclear morphological changes identified in ACC-MESO-1 cells after ablation of *BMAL1*. (*b*) IF of α-tubulin and DAPI stains. The upper panels represent ACC-MESO-1 cells treated with siRNA control. The lower panels represent the most frequent morphological changes (arrow indicates micronucleation and arrow head indicates multiple nuclei) in single ACC-MESO-1 cell after *BMAL1* depletion. The middle panels represent ACC-MESO-1 cells treated with *BMAL1* siRNA. (*c*) Quantification of the binuclear, multinuclear and micronuclear phenotypes in ACC-MESO-1 cells after BMAL1 knockdown. (*d*) Cell cycle profiling of ACC-MESO-1 cells showing marked decrease of *BMAL1*-induced cell death and polyploidy formation following mitosis block. ACC-MESO-1 cells transfected with *BMAL1* siRNA or control oligos with double-thymidine (black arrows) and without thymidine treatment (arrow heads) were harvested for analyses of DNA content by flow cytometry. Synchronized cells at late G1/early S by double-thymidine escaped from *BMAL1* knockdown-induced cell death with marked reduction in subG1 and polyploidy formation. (*e*) Time lapse microscopic examination showing the aberrant mitosis in ACC-MESO-1 cells transfected with *BMAL1* siRNA (white arrow head) and intact mitosis in cells transfected with control oligos (white arrow). (*f*) Proposed molecular mechanism of BMAL1 knockdown-induced mitotic catastrophe in ACC-MESO-1 cells. Decreasing cyclin B below a critical level results in mitosis skipping and enhances polyploidy formation. Downregulation of p21WAF1/CIP1 results in accumulation of cyclin E which could lead to increased number of polyploidy cells. Wee1 downregulation could contribute to eventual escape from G2/M arrest, which in turns participates in impairment of mitotic integrity. [Color figure can be viewed in the online issue, which is available at wileyonlinelibrary.com.]

MPM samples. Two out of three Stage IV-MPM patients were positive for BMAL1, whereas three out of 12 Stage III-MPM patients were positive (Table 1). This suggests that BMAL1 expression may be associated with advanced stage-MPM, but the small patients' number makes it difficult to draw a firm conclusion on this possible association (Supporting Information, Fig. S2). It would be of importance to analyze the association between BMAL1 expression and

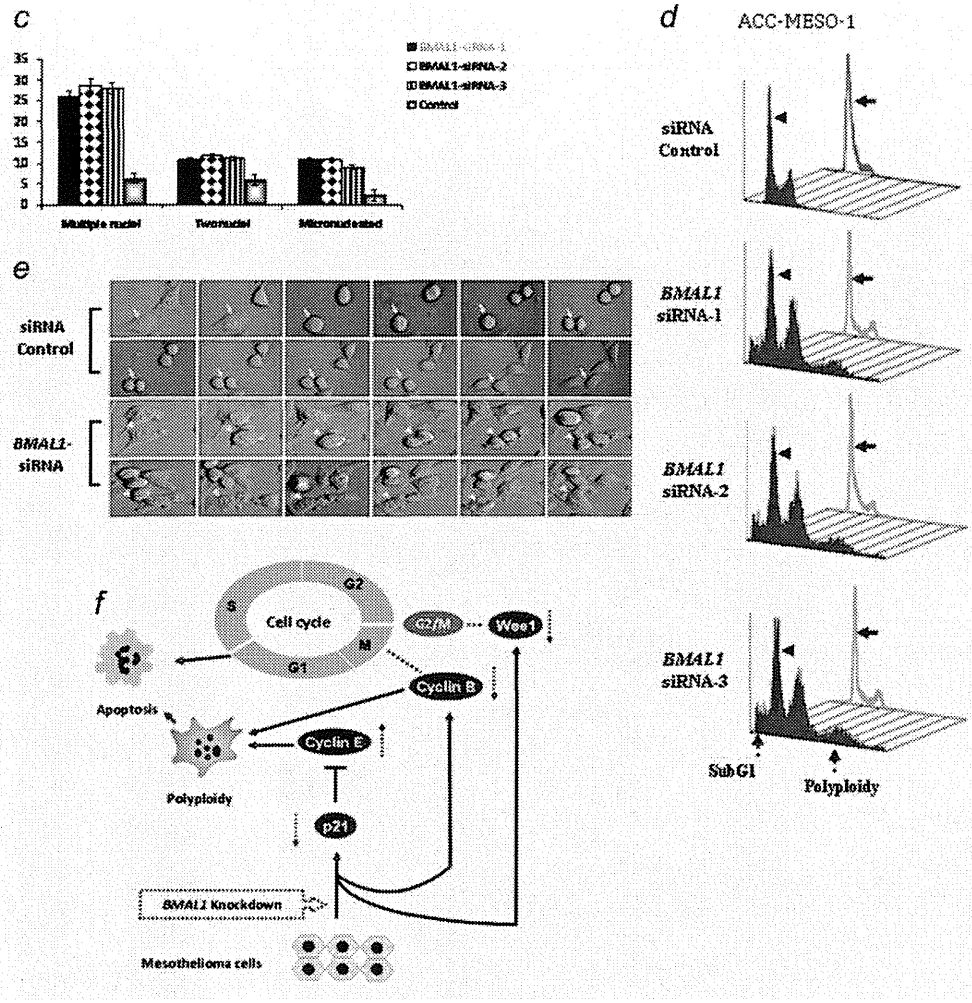

Figure 6. (Continued).

clinicopathological features of MPM using a large cohort. In line with our provisional results, high BMAL1 expression was observed in metastatic breast, colorectal and liver cancers,[12,13] these findings suggest that *BMAL1* has an oncogenic activities in a variety of human cancers.

A prior study reported that clock genes oscillation was found in different tissues including muscle, liver and adipose tissues.[24] *BMAL1* rhythmic expression was observed also in NIH3T3 cell following synchronization by serum shock.[25] Here, we found that the rhythmic expression of *BMAL1* over the 24 hr period was intact and clearly observed in NIH3T3 cells and MeT-5A as well. Intriguingly, ACC-MESO-1 cells showed constant levels of *BMAL1* mRNA. This result is consistent with a recent report[20] showing that *BMAL1* is rhythmically expressed in mouse prostate while serum-shocked synchronized prostate cancer cells showed disrupted circadian rhythmicity of *BMAL1* gene. In line with Roe *et al.*'s[15] results who reported that *BMAL1* was found to be overexpressed concomitantly with downregulation of its negative counterpart in MPM compared to the normal parietal pleural tissue, our findings support the notion that the circadian rhythm pathway could be deregulated in MPM.

We demonstrated that inhibition of *BMAL1* expression using RNAi technique significantly suppressed proliferation, anchorage-dependent and independent clonal growth in MPM cells. To explore how *BMAL1* knockdown induced growth inhibition, we performed apoptosis assays and found that depletion of *BMAL1* expression by siRNA resulted in a significant increase in the fraction of apoptotic and necrotic cells in the MPM cell lines (ACC-MESO-1 and H290) with limited effect in MeT-5A. We also examined the regulatory role of *BMAL1* in MPM cell cycle and its importance in sustained cell proliferation. Interestingly, we found that RNAi-mediated knockdown of *BMAL1* resulted in cell cycle disruption of ACC-MESO-1 cells but not in MeT-5A cells.

Following *BMAL1* transient knockdown, we observed multiple morphological abnormalities consistent with aberrant mitotic process. There was an increase of binucleated cells, which may correspond to the modest increase in the G2/M phase cell population. Furthermore, some other cells

(about 10%) showed micronucleation. Bergman *et al.*[26] reported that the occurrence of cells with double nucleus suggests that these cells undergo cell division without segregating their DNA and could be explained by the increase in cells with 4 *N* DNA content seen with flow cytometry. Importantly, micronucleation is highly indicative of mitotic catastrophe and could be resulted from chromosomal missegregation caused by DNA breaks. It is quite possible that ACC-MESO-1 cells underwent mitotic catastrophe due to impairment of cell cycle regulator proteins, such as, cyclin B, $p21^{WAF1/CIP1}$ and Wee1 (Fig. 6*f*). It is demonstrated that decreasing cyclin B below a critical level results in mitosis skipping and enhances polyploidy formation, which is considered as one of the characteristics of mitotic catastrophe.[27] Polyploidy cells pass an extra round of cell cycle and finally undergo apoptosis.[28] In addition, Wee1 downregulation could contribute to eventual escape from G2/M arrest, which in turns participates in impairment of mitotic integrity. In this study, we observed downregulation of $p21^{WAF1/CIP1}$ and cyclin E upregulation following *BMAL1* knockdown, and the latter could also lead to increased number of polyploidy cells. Other investigators noted that *BMAL1* modulate the transcriptional activity of p53 toward its target p21 and clearly showed that *BMAL1* knockdown caused a decrease in p21 level.[22] Moreover, a previous study reported that overexpression of cyclin E led to impairment of mitosis and polyploidy formation.[29] We believe that accumulation of polyploidy, large multinucleated cells and micronucleation in ACC-MESO-1 after *BMAL1* knockdown were consistent with cell death mechanism involving mitotic catastrophe. It has been shown that mitotic catastrophe could be considered as an important safeguard to prevent the proliferation of polyploidy cells[30] and apoptosis frequently follows mitotic catastrophe.[31] Taken together, these findings show that *BMAL1* plays a critical role in the mitotic process of cancer cells. To our knowledge, this study is the first to shed light on the involvement of *BMAL1* in polyploidy formation, impairment of mitotic events, and also to highlight the role of circadian clock genes in MPM. In conclusion, we provide evidence that BMAL1 plays an important role and it may be a promising therapeutic target for MPM, but careful consideration is needed to avoid the counter effect on tissues dependant on BMAL1 such as muscles and liver.

References

1. Robinson BW, Musk AW, Lake RA. Malignant mesothelioma. *Lancet* 2005;366:397–408.
2. Sekido Y. Molecular biology of malignant mesothelioma. *Environ Health Prev Med* 2008;13: 65–70.
3. Tsao AS, Wistuba I, Roth JA, et al. Malignant pleural mesothelioma. *J Clin Oncol* 2009;27: 2081–90.
4. Taniguchi H, Fernandez AF, Setien F, et al. Epigenetic inactivation of the circadian clock gene *BMAL1* in hematologic malignancies. *Cancer Res* 2009;69:8447–54.
5. Balsalobre A, Damiola F, Schibler U. A serum shock induces circadian gene expression in mammalian tissue culture cells. *Cell* 1998;93: 929–37.
6. Straif K, Baan R, Grosse Y, et al. Carcinogenicity of shift-work, painting, and fire-fighting. *Lancet Oncol* 2007;8:1065–6.
7. Canaple L, Kakizawa T, Laudet V. The days and nights of cancer cells. *Cancer Res* 2003;63: 7545–52.
8. Bunger MK, Wilsbacher LD, Moran SM, et al. Mop3 is an essential component of the master circadian pacemaker in mammals. *Cell* 2000;103: 1009–17.
9. Gauger MA, Sancar A. Cryptochrome, circadian cycle, cell cycle checkpoints, and cancer. *Cancer Res* 2005;65:6828–34.
10. Matsuo T, Yamaguchi S, Mitsui S, et al. Control mechanism of the circadian clock for timing of cell division in vivo. *Science* 2003;302: 255–9.
11. Fu L, Lee CC. The circadian clock: pacemaker and tumour suppressor. *Nat Rev Cancer* 2003;3: 350–61.
12. Oshima T, Takenoshita S, Akaike M, et al. Expression of circadian genes correlates with liver metastasis and outcomes in colorectal cancer. *Oncol Rep* 2011;25:1439–46.
13. Kuo SJ, Chen ST, Yeh KT, et al. Disturbance of circadian gene expression in breast cancer. *Virchows Arch* 2009;454:467–74.
14. Koyanagi S, Kuramoto Y, Nakagawa H, et al. A molecular mechanism regulating circadian expression of vascular endothelial growth factor in tumor cells. *Cancer Res* 2003;63:7277–83.
15. Roe OD, Anderssen E, Helge E, et al. Genome-wide profile of pleural mesothelioma versus parietal and visceral pleura: the emerging gene portrait of the mesothelioma phenotype. *PLoS One* 2009;4:e6554.
16. Usami N, Fukui T, Kondo M, et al. Establishment and characterization of four malignant pleural mesothelioma cell lines from Japanese patients. *Cancer Sci* 2006;97:387–94.
17. Takeyama Y, Sato M, Horio M, et al. Knockdown of *ZEB1*, a master epithelial-to-mesenchymal transition (EMT) gene, suppresses anchorage-independent cell growth of lung cancer cells. *Cancer Lett* 2010;296:216–24.
18. Husain AN, Colby TV, Ordonez NG, et al. Guidelines for pathologic diagnosis of malignant mesothelioma: a consensus statement from the International Mesothelioma Interest Group. *Arch Pathol Lab Med* 2009;133:1317–31.
19. Sato M, Vaughan MB, Girard L, et al. Multiple oncogenic changes (K-RAS(V12), p53 knockdown, mutant EGFRs, p16 bypass, telomerase) are not sufficient to confer a full malignant phenotype on human bronchial epithelial cells. *Cancer Res* 2006;66:2116–28.
20. Cao Q, Gery S, Dashti A, et al. A role for the clock gene per1 in prostate cancer. *Cancer Res* 2009;69:7619–25.
21. Grechez-Cassiau A, Rayet B, Guillaumond F, et al. The circadian clock component BMAL1 is a critical regulator of p21WAF1/CIP1 expression and hepatocyte proliferation. *J Biol Chem* 2008; 283:4535–42.
22. Mullenders J, Fabius AW, Madiredjo M, et al. A large scale shRNA barcode screen identifies the circadian clock component ARNTL as putative regulator of the p53 tumor suppressor pathway. *PLoS One* 2009;4:e4798.
23. Wood PA, Du-Quiton J, You S, et al. Circadian clock coordinates cancer cell cycle progression, thymidylate synthase, and 5-fluorouracil therapeutic index. *Mol Cancer Ther* 2006;5: 2023–33.
24. Yang X, Downes M, Yu RT, et al. Nuclear receptor expression links the circadian clock to metabolism. *Cell* 2006;126:801–10.
25. Yagita K, Tamanini F, van Der Horst GT, et al. Molecular mechanisms of the biological clock in cultured fibroblasts. *Science* 2001;292: 278–81.
26. Bergman LM, Birts CN, Darley M, et al. CtBPs promote cell survival through the maintenance of mitotic fidelity. *Mol Cell Biol* 2009;29:4539–51.
27. Galimberti F, Thompson SL, Ravi S, et al. Anaphase catastrophe is a target for cancer therapy. *Clin Cancer Res* 2011;17:1218–22.
28. Li S, Szymborski A, Miron MJ, et al. The adenovirus E4orf4 protein induces growth arrest and mitotic catastrophe in H1299 human lung carcinoma cells. *Oncogene* 2009;28:390–400.
29. Keck JM, Summers MK, Tedesco D, et al. Cyclin E overexpression impairs progression through mitosis by inhibiting APC(Cdh1). *J Cell Biol* 2007;178:371–85.
30. Marrazzo E, Marchini S, Tavecchio M, et al. The expression of the DeltaNp73beta isoform of p73 leads to tetraploidy. *Eur J Cancer* 2009;45: 443–53.
31. Rivera A, Mavila A, Bayless KJ, et al. Cyclin A1 is a p53-induced gene that mediates apoptosis, G2/M arrest, and mitotic catastrophe in renal, ovarian, and lung carcinoma cells. *Cell Mol Life Sci* 2006;63:1425–39.